Enhanced diphoton rates at Fermi and the LHC

Kai Schmidt-Hoberg[a], **Florian Staub**[b], **Martin Wolfgang Winkler**[c]

[a] *Theory Division, CERN, 1211 Geneva 23, Switzerland*

[b] *Bethe Center for Theoretical Physics & Physikalisches Institut der Universität Bonn, Nußallee 12, 53115 Bonn, Germany*

[c] *Deutsches Elektronen-Synchrotron DESY, Notkestraße 85, D-22607 Hamburg, Germany*

Abstract

We show that within MSSM singlet extensions the experimental hints beyond the standard model from the Fermi LAT telescope as well as from the LHC can be explained simultaneously while being consistent with all experimental constraints. In particular we present an example point which features a ~ 130 GeV lightest neutralino with an annihilation cross section into photons consistent with the indication from the Fermi satellite with simultaneously the right relic abundance, a continuum photon spectrum consistent with observation, direct detection cross section below the experimental limits, electroweak observables consistent with experiment and a 125 GeV light Higgs boson with a slightly enhanced $h \rightarrow \gamma\gamma$ rate.

1   Introduction

2012 has been a very intriguing year regarding hints for new physics, both at the LHC and the Fermi large area telescope. While the data from ATLAS [1] and CMS [2] feature a new bosonic state with mass $m \sim 125$ GeV which is consistent with the expectation from a standard model (SM) Higgs, both experiments see indications for an excess in the diphoton channel. This potential enhancement in the diphoton rate has attracted much attention recently, see e.g. [3–20]. In contrast the diboson decays into WW^* and ZZ^* seem to be in accord with the SM expectation, which make explanations of the enhanced diphoton rate due to an increased partial decay width particularly appealing.

A similarly exciting topic this year have been the hints for a γ-ray line in the Fermi LAT data as reported in [21, 22]. γ ray lines are considered the smoking gun of annihilating dark matter, as astrophysical processes able to induce line-like features are very rare (see however [23, 24]). Intriguingly, the morphology of the excess is consistent with the expected distribution of dark matter up to a small offset from the galactic center [25, 26].[1] Currently the data are being re-analysed by the Fermi collaboration, and there seems to be an indication of a line-like feature at a slightly higher energy of 135 GeV [28], where the shift results from a reprocessing of the data. The statistical significance of the excess found by the Fermi collaboration is, however, not as high as claimed in [22, 25, 29], although this also depends on the target region considered. A line feature has also appeared in the γ ray data of the earth limb, raising some concerns about an instrumental effect [28, 30, 31]. Radio telescopes might help to confirm or rule out the dark matter interpretation of the line soon [32]. While the origin of the γ-ray line from the galactic center still has to be clarified, a noticeable amount of theoretical interest has been triggered [33–49]. If interpreted in terms of dark matter, the γ-ray line requires a rather large annihilation cross section into photons, $\langle \sigma v \rangle_{\gamma\gamma} \sim 10^{-27}$ cm^3 s^{-1}, if one assumes an Einasto profile [22]. Such a large cross section was found to be very difficult to accommodate in particle physics models, especially as the Fermi data are consistent with pure background at lower energies, i.e. competing annihilation channels must be sufficiently suppressed [42, 47, 50, 51].

While one may tackle each of these experimental anomalies individually, it is intriguing to speculate about a possible common origin. In this article we show that the signals from both Fermi and the LHC can be explained simultaneously within singlet extensions of the MSSM, while being consistent with all experimental constraints. Singlet extensions are particularly interesting given the observed value for the Higgs mass

---

[1]Recent numerical simulations indicate that such a small offset can indeed be realized in realistic models of galaxy formation [27].

because the electroweak fine-tuning can be substantially alleviated in these models. A somewhat generalised version of the NMSSM, the GNMSSM [52], which is based on a discrete R symmetry [53,54], was found to be particularly promising in this context [55]. In [19] it was found that in this setup the coupling of the CP even neutral light Higgs to light charginos can be strongly enhanced, leading to a sizeable increase in the $h \to \gamma\gamma$ rate. Interestingly the same coupling can lead to a rather large neutralino annihilation cross section into photons as indicated by the Fermi data, while being compatible with bounds from direct detection, electroweak precision observables, the continuum photon spectrum and with a 125 GeV Higgs with an enhanced diphoton rate.

This article is organised as follows: In the next section we will briefly review some aspects of the GNMSSM. In section 3 we will then discuss neutralino annihilation within this framework, before we come to constraints arising from the requirement of the correct relic abundance and the continuum photon spectrum in section 4. Constraints from direct and indirect detection experiments are analysed in section 5. Section 6 is then devoted to a thorough numerical study of a benchmark point, while section 7 contains our summary. Some useful information about the GNMSSM is collected in the appendix.

2 The GNMSSM

As a framework, we consider the GNMSSM, a generalised version of the NMSSM, which has a superpotential of the form

$$\mathcal{W} = \mathcal{W}_{\text{Yukawa}} + \frac{1}{3}\kappa S^3 + (\mu + \lambda S)H_u H_d + \frac{1}{2}\mu_s S^2 \; . \tag{1}$$

Here $\mathcal{W}_{\text{Yukawa}}$ are the MSSM superpotential terms generating the usual Yukawa couplings and we used the freedom to shift the singlet S to set a potential linear term in S to zero. This superpotential has additional explicit mass terms μ and μ_s which are not present in the $\mathbb{Z}_3$ symmetric NMSSM which is usually considered (for reviews of the NMSSM see e.g. [56,57]). While the apparent un-naturalness of these additional mass terms has prevented a larger community from studying the phenomenology of the GNMSSM, it has recently been realised that exactly this structure naturally arises from an underlying R symmetry as discussed in [54]. The fact that this R symmetry also eliminates the dangerous dimension four and five baryon- and lepton-number violating terms and avoids destabilising tadpoles and domain wall problems makes it a more promising starting point than the $\mathbb{Z}_3$ symmetric NMSSM.

The soft SUSY breaking terms associated with the extended Higgs sector of the

GNMSSM are given by

$$V_{\text{soft}} = m_s^2 |s|^2 + m_{h_u}^2 |h_u|^2 + m_{h_d}^2 |h_d|^2$$
$$+ \left(b\mu \, h_u h_d + \lambda A_\lambda s h_u h_d + \frac{1}{3}\kappa A_\kappa s^3 + \frac{1}{2}b_s s^2 + \xi_s s + h.c. \right) . \tag{2}$$

The resulting mass matrices as well as the relevant couplings for our discussion are given in appendix A and B. The field content is the same as in the NMSSM. In comparison with the MSSM there is an additional singlet fermion which mixes into the neutralino sector and an additional complex scalar which mixes into the Higgs sector. For more details on the model, see [52, 55].
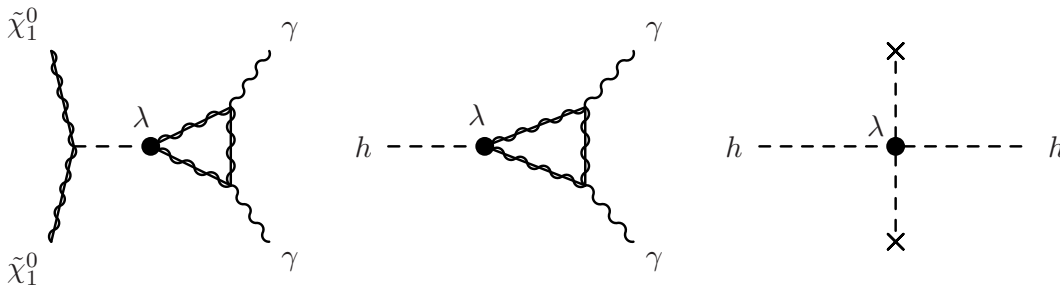

Figure 1: In the GNMSSM the λ-coupling drives the annihilation of neutralinos into photons (left), enhances the Higgs decay rate into photons (middle) and provides an additional contribution to the Higgs boson mass (right).

The Higgs sector of the GNMSSM has been discussed in [19,52,55]. As in the NMSSM there is an additional tree-level contribution to the lightest Higgs mass, which is large for small $\tan\beta$ and large λ, allowing to evade the upper bound of $m_h < M_Z$ present in the MSSM. The fact that radiative corrections due to top/stop loops are no longer needed drastically reduces the electroweak fine-tuning in MSSM singlet extensions [58–62] for large values of λ. Given the Higgs mass of 125 GeV the GNMSSM has been shown to be particularly interesting in this context [52, 55]. One additional advantage of the GNMSSM is the fact that for small v_s no tuning in the Higgs mass matrix is required to avoid large doublet-singlet mixing[2]. It has also been argued that allowing even larger values of λ, relaxing the condition that it remain perturbative up to the GUT scale, leads to an additional reduction in the fine-tuning [63].

---

[2] In the NMSSM it is common practice to tune the parameter A_λ such that the off-diagonal entry in the mass matrix is close to zero, avoiding doublet-singlet mixing and allowing for a correspondingly larger Higgs mass.

As discussed in [19] scenarios with large λ may also accommodate an enhanced diphoton rate as observed by ATLAS and CMS: in addition to the dominant W and top loops present in the SM, new sizeable contributions from charged Higgs and chargino loops can arise, if these states are light. While a light charged Higgs is generically challenged by the measurement of $b \to s\gamma$, a light chargino is perfectly viable and an interesting possibility. In the next section we will show that large λ and light charginos can also lead to a large annihilation cross section into photons, see also figure 1.

3 Neutralino annihilation into photons

The mass matrix as well as the relevant couplings of the GNMSSM neutralino sector can be found in the appendix. Compared to the MSSM, the GNMSSM offers two alterna-
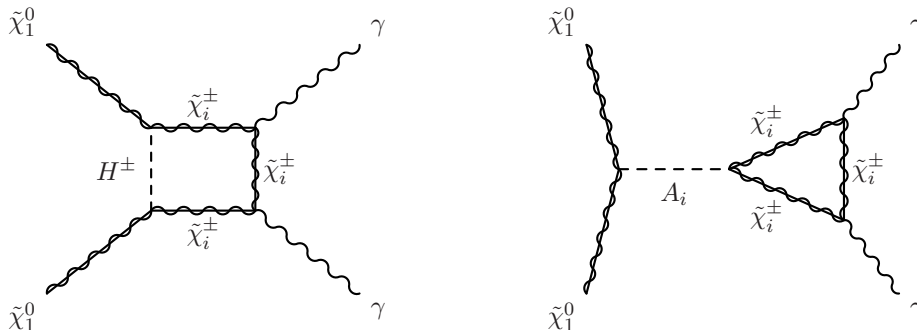

Figure 2: Relevant Feynman diagrams for annihilation of the lightest neutralino into two photons within the GNMSSM.

tive possibilities to achieve a large annihilation cross section $\langle\sigma v\rangle_{\gamma\gamma}$. The corresponding Feynman diagrams are shown in figure 2. In case $\tilde{\chi}_1^0$ carries a sizeable singlino fraction, the chargino/ charged Higgs loop on the left experiences a drastic enhancement compared to the MSSM through the λ-coupling. However, even for $\lambda > 1$, a cross section large enough to explain the Fermi line requires not only the charginos but also the charged Higgs bosons to be very light. This typically causes problems with flavour observables, in particular $b \to s\gamma$. Therefore, we will concentrate on the second possibility in the following, shown in the right panel of figure 2. The diagram contains a pseudoscalar Higgs A_i in the s-channel, i.e. the cross section can be enhanced in the vicinity of the pseudoscalar resonance (see also [44]).

Analytically, one finds (see e.g. [64, 65])

$$\langle\sigma v\rangle_{\gamma\gamma} = \frac{\alpha^2 m_{\tilde{\chi}_1^0}^2}{16\pi^3}\left|\,\tilde{\mathcal{A}}\,\right|^2 \,. \tag{3}$$

with

$$\tilde{\mathcal{A}}_{A_1} = \sum_{\tilde{\chi}_i^\pm} \frac{m_{\tilde{\chi}_i^\pm}}{2\, m_{\tilde{\chi}_1^0}} \frac{g_{\tilde{\chi}_1^0 \tilde{\chi}_1^0 A_1}\, g_{\tilde{\chi}_i^\pm \tilde{\chi}_i^\pm A_1}}{(4\, m_{\tilde{\chi}_1^0}^2 - m_{A_1}^2)} \, \arctan^2\left[\left(\frac{m_{\tilde{\chi}_i^\pm}^2}{m_{\tilde{\chi}_1^0}^2} - 1\right)^{-1/2}\right] . \tag{4}$$

Here $g_{\tilde{\chi}_1^0 \tilde{\chi}_1^0 A_1} \equiv g_{\tilde{\chi}_1^0 \tilde{\chi}_1^0 A_1}^R - g_{\tilde{\chi}_1^0 \tilde{\chi}_1^0 A_1}^L$ and $g_{\tilde{\chi}_i^\pm \tilde{\chi}_i^\pm A_1} \equiv g_{\tilde{\chi}_i^\pm \tilde{\chi}_i^\pm A_1}^L - g_{\tilde{\chi}_i^\pm \tilde{\chi}_i^\pm A_1}^R$. The general form of the trilinear couplings $g_{\tilde{\chi}_1^0 \tilde{\chi}_1^0 A_1}^{L,R}$ and $g_{\tilde{\chi}_i^\pm \tilde{\chi}_i^\pm A_1}^{L,R}$ is given in appendix B. Throughout this article we will assume λ and κ to be real.

An interesting limit arises if we assume that $\tilde{\chi}_1^0$ and A_1 are dominantly singlet-like. In this case, we obtain $g_{\tilde{\chi}_1^0 \tilde{\chi}_1^0 A_1} = \sqrt{2}\kappa$. Further, only the higgsino-like chargino couples to A_1 with $g_{\tilde{\chi}_1^\pm \tilde{\chi}_1^\pm A_1} = \lambda/\sqrt{2}$ for the lighter chargino being a pure higgsino. Setting as an example $m_{\tilde{\chi}_1^\pm} = 1.5\, m_{\tilde{\chi}_1^0}$, we obtain in this limit

$$\langle \sigma v \rangle_{\gamma\gamma} \simeq (6 \cdot 10^{-28}\ \mathrm{cm^3\ s^{-1}}) \cdot \lambda^2 \kappa^2 \left(\frac{(100\ \mathrm{GeV})^2}{4\, m_{\tilde{\chi}_1^0}^2 - m_{A_1}^2}\right)^2 \left(\frac{m_{\tilde{\chi}_1^0}}{130\ \mathrm{GeV}}\right)^2 . \tag{5}$$

This shows that a cross section large enough to explain the Fermi line can indeed be realised if we allow for a mild tuning of m_{A_1}. In the above example, m_{A_1} has to be within the range $m_{A_1} \simeq 240 - 280\ \mathrm{GeV}$ (if we assume $\lambda, \kappa \lesssim 1$). The tuning is, however, substantially less severe than in the NMSSM case [44]. The reason is that in the NMSSM it is not possible to obtain a dominantly singlet like pseudoscalar and a singlino like LSP with the desired masses simultaneously. Instead the lightest neutralino has to be predominantly bino like, leading to much smaller effective couplings. Large enough annihilation cross sections can only be achieved very close to the pseudoscalar resonance, which in turn requires substantial tuning, in particular, when the most recent XENON100 bounds [66] are taken into account, which appeared after [44] was published.

In addition to the γ ray line from annihilation into two photons, there is a second line from the process $\tilde{\chi}_1^0 \tilde{\chi}_1^0 \to Z\gamma$ at a slightly lower energy

$$E_\gamma = m_{\tilde{\chi}_1^0} \left(1 - \frac{M_Z^2}{4\, m_{\tilde{\chi}_1^0}^2}\right) . \tag{6}$$

As has been shown in [25] such a double line structure even slightly improves the fit to the Fermi data compared to a single line. The cross section $\langle \sigma v \rangle_{Z\gamma}$ can be calculated with the formulas presented in [67]. We find that for a pure higgsino $\langle \sigma v \rangle_{Z\gamma} / \langle \sigma v \rangle_{\gamma\gamma} \sim 0.6$. The wino, however, has a stronger coupling to Z bosons than the higgsino. Therefore, chargino mixing tends to increase the relative importance of the $Z\gamma$-channel.

4 Continuum photons and relic density

Even if dark matter annihilations induce a γ ray line consistent with Fermi, it remains quite challenging not to overproduce continuum γs by competing annihilation processes. Irrespective of whether dark matter is produced thermally or non-thermally, its present-day annihilation fraction into γs must satisfy [47]

$$\text{Br}_{\gamma\gamma} = \frac{\langle\sigma v\rangle_{\gamma\gamma}}{\langle\sigma v\rangle} \gtrsim 10^{-2} \ . \tag{7}$$

For the winos and higgsinos of the MSSM, this fraction is in the range $\text{Br}_{\gamma\gamma} = \mathcal{O}(10^{-3})$. Therefore, the low energy γ data disfavour an explanation of the Fermi line within the framework of the MSSM [47, 50].

In the GNMSSM there is a simple possibility to suppress the continuum γs. As in [44], we take the lighter pseudoscalar A_1 to be an almost pure singlet. With the appropriate choice of $b\mu$ and b_s it is simple to arrive at a situation where the singlet pseudoscalar remains light while the MSSM pseudoscalar becomes heavy and decouples. In this case, any tree level annihilation process into quarks through an intermediate A_1 is suppressed by the mixing angle between singlet and MSSM pseudoscalar. More specifically, for $\lambda \sim 1$ the effective coupling of A_1 to photons becomes comparable to the tree-level coupling to bottom quarks for a doublet fraction at the level of 0.1%. This can easily be achieved for a sufficiently heavy A_2 without requiring any cancellations in the pseudoscalar mass matrix.

Competing annihilation processes into SM states which do not proceed through A_1 can be suppressed if $\tilde{\chi}_1^0$ is dominantly singlino-like. A singlino-like LSP arises if the gauginos and higgsinos are sufficiently heavier than the singlino. With a singlino-like $\tilde{\chi}_1^0$ and a singlet-like A_1 one naturally obtains $\text{Br}_{\gamma\gamma} \gg 10^{-2}$.

Within the GNMSSM it is also possible to realise thermal dark matter and the γ ray line simultaneously. Thermal production requires a total neutralino annihilation cross section $\langle\sigma v\rangle_{\text{FO}} \sim 2 \cdot 10^{-26}$ cm^3 s^{-1} at the time of freeze-out. This can e.g. be achieved through a subdominant wino admixture in $\tilde{\chi}_1^0$ which induces annihilation into W bosons. Alternatively, a thermal cross section can be realised by the annihilation of $\tilde{\chi}_1^0$ into bottom quarks or gluons through the MSSM admixture of A_1.

In figure 3 we present the γ ray flux for a specific benchmark choice of the GNMSSM parameters which can be found in table 1. The benchmark scenario will be discussed in more detail in section 6. For the dark matter density distribution we assume an Einasto profile with the parameters as given in [22]. The Fermi data are taken from region 4 (source) of the same reference. The γ ray lines from dark matter annihilation into $\gamma\gamma$
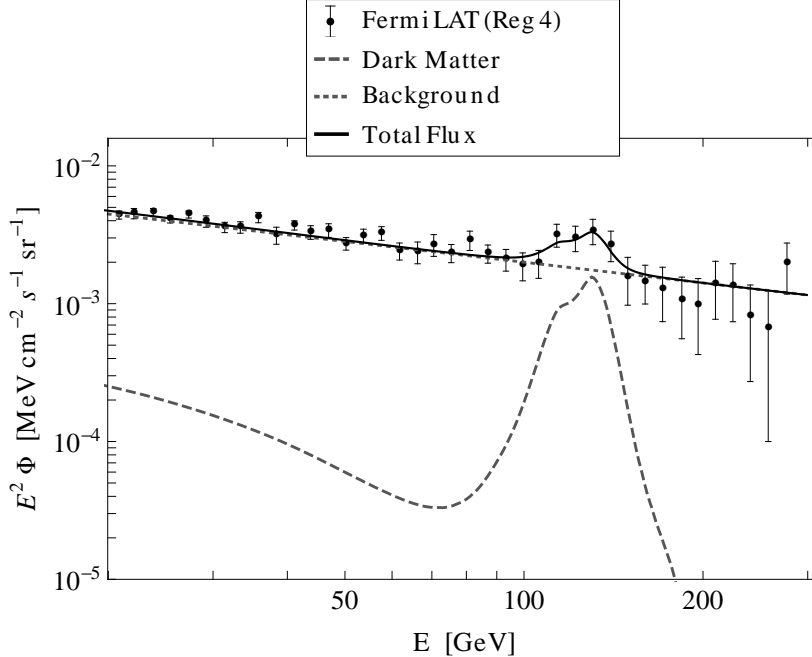
Figure 3: γ ray flux for the benchmark scenario of table 1. The Fermi data are taken from [22] (region 4, source). The dark matter induced flux comprises the lines from annihilation into $\gamma\gamma$ and γZ as well as the continuum photons from the fragmentation and decay of the accompanying annihilation products. The background is modelled with a power law.

and $Z\gamma$ have been convoluted with the Fermi energy resolution as extracted from table 3 in [22]. The γ ray background is modeled with a featureless power law with index -2.5.

It can be seen that the double line at $E = 130\,\mathrm{GeV}$ and $E = 114\,\mathrm{GeV}$ (from annihilation into $\gamma\gamma$ and $Z\gamma$ respectively) gives a very good fit to the data. The continuum γs which – in the benchmark scenario – mainly arise from the WW-channel are sufficiently suppressed, i.e. they are nicely consistent with the low energy data.

5 Direct and indirect detection constraints

Let us now briefly discuss constraints on the model which arise from direct dark matter searches. The spin-independent cross section of the lightest neutralino with nucleons σ_n^{SI} is typically dominated by exchange of the light scalar Higgs h_1. It can be written in

the form[3]

$$\sigma_n^{\rm SI} \simeq \frac{4\,m_n^4}{\pi}\,|f_q|^2\,\left(f_u^n + f_d^n + f_s^n + \frac{6}{27}\,f_G^n\right)^2 ,$$

(8)

where f_u^n, f_d^n, f_s^n and f_G^n denote the up-, down-, strange-quark and gluon contributions to the nucleon mass m_n which we take from [68]. For simplicity, we have applied the decoupling limit on the MSSM Higgs fields such that the effective neutralino quark coupling divided by the quark mass f_q is universal among the quark families. The latter takes the form (see e.g. [69])

$$|f_q|^2 = \frac{G_F}{2\sqrt{2}\,m_{h_1}^4}\,\left|g_{\tilde\chi_1^0\tilde\chi_1^0 h_1}\right|^2\,\left(1 - Z_{13}^{H\,2}\right) ,$$

(9)

where G_F is the Fermi constant and $Z_{13}^{H\,2}$ the singlet fraction of the light Higgs h_1 (see appendix A). The neutralino Higgs coupling is given as $g_{\tilde\chi_1^0\tilde\chi_1^0 h_1} = g_{\tilde\chi_1^0\tilde\chi_1^0 h_1}^R + g_{\tilde\chi_1^0\tilde\chi_1^0 h_1}^L$ with the left and right couplings being defined in appendix B. Note that they depend strongly on the composition of the lightest neutralino.

The relevant limit on the cross section $\sigma_n^{\rm SI}$ is set by the XENON100 experiment, which for a neutralino mass $m_{\tilde\chi_1^0} \simeq 130\,{\rm GeV}$ corresponds to [66]

$$\sigma_n^{\rm SI} \leq 3\cdot 10^{-45}\,{\rm cm}^2 .$$

(10)

By use of (9) we can translate this into a limit on the coupling $g_{\tilde\chi_1^0\tilde\chi_1^0 h_1}^{L,R}$. Assuming that h_1 is dominantly SM like, we estimate $|g_{\tilde\chi_1^0\tilde\chi_1^0 h_1}| \lesssim 0.05$.[4]

As described in section 4, we are mainly interested in the case where $\tilde\chi_1^0$ is singlino-like such that the production of continuum γs is suppressed. However, in order to enhance annihilation of $\tilde\chi_1^0$ into photon pairs, it is favourable to have light (charged) higgsinos. Thus $\tilde\chi_1^0$ always contains a non-negligible higgsino admixture. In this case $g_{\tilde\chi_1^0\tilde\chi_1^0 h_1}$ typically receives comparable contributions through the λ as well as the κ coupling bearing also the possibility of (partial) cancellations. Still, we find that for $\lambda \sim 1$ the higgsino fraction of $\tilde\chi_1^0$ should not exceed $\sim 10\%$ in order to satisfy the XENON bound.

Further constraints on the model arise from the neutrino searches by Super-Kamiokande [70, 71] and IceCube [72] which aim to detect the annihilation of dark matter particles in the sun. They provide especially strong bounds on the spin-dependent cross section $\sigma_p^{\rm SD}$ of WIMPs with protons. Assuming $m_{\tilde\chi_1^0} \simeq 130\,{\rm GeV}$, the relevant upper limit reads $\sigma_p^{\rm SD} = 4\cdot 10^{-40}\,{\rm cm}^2$ [70] if the LSPs dominantly annihilate into W bosons. The

---

[3]We neglect the small differences between proton and neutron.
[4]Note, however, that the uncertainties in the nucleon composition may affect this constraint.

constraint, however, gets significantly weaker for annihilation channels which induce a softer neutrino spectrum. In the considered region of parameter space, the leading spin-dependent WIMP proton cross section σ_p^{SD} arises from Z exchange. It scales with the higgsino components of $\tilde{\chi}_1^0$, more specifically $\sigma_p^{\mathrm{SD}} \propto |N_{13}|^2 - |N_{14}|^2$ (cf. appendix B). While this cross-section can be sizeable, there generically occur cancellations due to $|N_{13}| \sim |N_{14}|$. The most dangerous situation arises if $\tilde{\chi}_1^0$ is strongly mixed among the different states as in this case N_{13} and N_{14} typically get split. Then, a σ_p^{SD} close to the current experimental bounds may be generated.

We find that the remaining constraints from indirect dark matter detection, arising e.g. from γ ray searches in the Milky Way satellite galaxies by Fermi [73] or antiproton searches by PAMELA [74, 75] and BESS-Polar II [76, 77], are in general weaker than those from the continuum γs studied previously. To illustrate that in the GNMSSM, the Fermi line can be explained while all direct and indirect detection constraints are satisfied, we provide an explicit example in the next section.

6　A benchmark scenario

After we have gained some analytical understanding, we now turn to a full-fledged numerical analysis. For this purpose we use the `SPheno` version [78, 79] for the GNMSSM created by `SARAH` [80–83] which has been presented in [55]. This version performs a complete one-loop calculation of all SUSY and Higgs masses [84, 85] and includes the dominant two-loop corrections for the scalar Higgs masses [86–89]. In addition, it calculates the decay widths and branching ratios of all SUSY and Higgs particles. In the Higgs sector the decays are calculated with the following precision: the channels with two SUSY particles, SM leptons or SM vector bosons in the final state are calculated at tree level. In contrast, for quark final states the dominant one-loop QCD corrections due to gluons are included [90]. For the decays into two photons and two gluons induced at one-loop level all possible leading order contributions are included. In addition, for the CP even Higgs also the dominant NLO QCD corrections are added [90]. Furthermore, this `SPheno` version also includes routines to calculate $b \to s\gamma$, $\delta\rho$ and $g-2$ which have been used to check possible constraints from these observables. These calculations are performed in the GNMSSM with the same precision as described in Ref. [79] for the MSSM.

For the calculation of the relic density of the lightest neutralino as well as to obtain $\langle \sigma v \rangle_{\gamma\gamma}$ we have used `MicrOmegas` [91–93]. For this purpose we created model files for `CalcHep` [94] with `SARAH`. These model files include optionally also the effective interactions $h_i\gamma\gamma$ and $A_i^h\gamma\gamma$. The numerical values for these operators as well as of all other
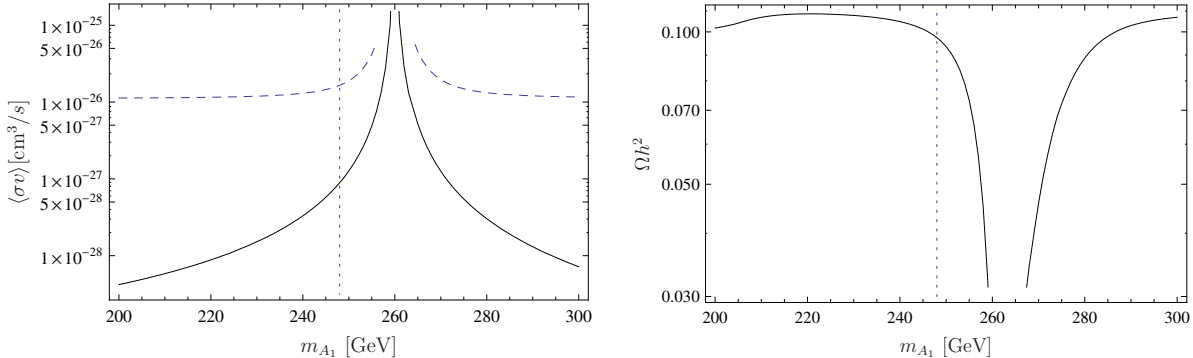
Figure 4: Left: The present day diphoton rate $\langle\sigma v\rangle_{\gamma\gamma}$ (solid line) and the total cross section $\langle\sigma v\rangle$ (dashed line) as function of the light pseudoscalar mass m_{A_1}. Right: dependence of the dark matter relic density Ωh^2 on the pseudoscalar mass. The other parameters are those of the point given in table 1. The dotted, vertical line indicates the pseudoscalar mass for our benchmark point.

parameters are read from the spectrum file written by `SPheno` using the `SLHA+` function-ality of `CalcHep` [95]. We also used `MicrOmegas` to calculate the continuous γ spectrum which has already been discussed in section 4.

In table 1 we show a benchmark point with all the desired features: the light Higgs mass is close to 125 GeV and the branching ratios into two photons is enhanced by 20% because of the chargino loop contributions. The LSP is the lightest neutralino which is mostly singlino-like and has a mass of 130 GeV. A mostly singlino LSP can be achieved by appropriate values for M_1, M_2 and μ_{eff}. While M_1 plays only a subleading role as long as the bino is heavier than the singlino, the choice of μ_{eff} has to be done more carefully: on the one hand it should not be too small in order to suppress the mixing between the singlino and higgsino, because a sizeable higgsino fraction is often in conflict with direct detection measurements. On the other hand, light charginos with a sizeable higgsino fraction are needed in order to enhance the loop contributions to $h \to \gamma\gamma$ and $\langle\sigma v\rangle_{\gamma\gamma}$. For the benchmark point a light chargino has been realized by a comparably small value of M_2, which however leads to a large mixing in the chargino sector. Note that the benchmark scenario is consistent with direct chargino searches at the LHC as the latter have only gained sensitivity to spectra with $m_{\tilde{\chi}_1^0} \lesssim 100\,\text{GeV}$ [97, 98].[5] The correct relic density is obtained mainly via annihilation into W^+W^-, while today's annihilation into photons mainly proceeds via the pseudoscalar exchange. This pseudoscalar is nearly a

---

[5]The sensitivity of chargino searches increases if there exists a slepton with mass between $m_{\tilde{\chi}_1^+}$ and $m_{\tilde{\chi}_1^0}$. This is, however, not the case in our benchmark scenario.

pure singlet and it is not necessary to be very close to the resonance: even with a mass more than 10 GeV away from the resonance the diphoton rate is enhanced to a level sufficient to explain the tentative Fermi line. This is a big improvement in comparison to the NMSSM where one has to be usually very close to the resonance: for cases with the pseudoscalar component of the singlet in the correct mass range, the singlino fraction of the LSP is very small and the coupling between both is highly suppressed. This is not only a drawback of the NMSSM with respect to the needed fine-tuning, but, what is even more important, this scenario is also under big pressure from direct detections bounds. The dependence of $\langle \sigma v \rangle$ on m_{A_1} is shown in figure 4 (left), with all other parameters as given in table 1. In the right panel we also show the relic density Ωh^2, which in the region of interest is hardly effected by the pseudoscalar resonance.

In order to illustrate the constraints on the parameter space of the GNMSSM which arise from direct and indirect detection, we show the results of a scan over μ and M_2 in figure 5. For each combination (μ, M_2) we adjusted the parameters μ_s and b_s such that $m_{\tilde{\chi}_1^0}$ and m_{A_1} remain fixed at their values from table 1. The remaining parameters were taken from the same table.
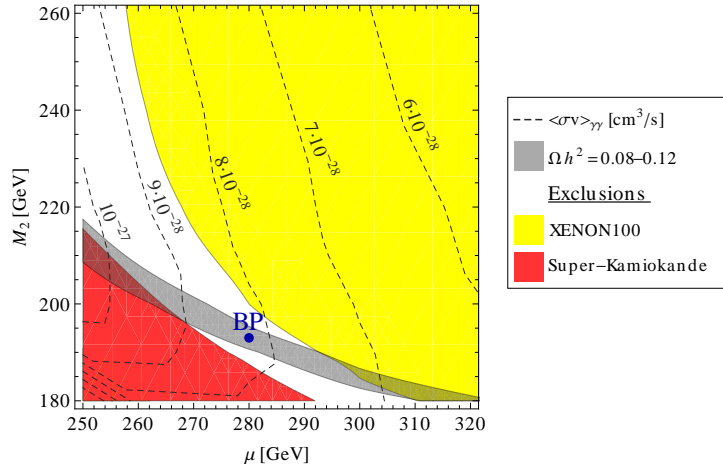
Figure 5: Parameter Scan in the GNMSSM (see text) with contours referring to the value of $\langle \sigma v \rangle_{\gamma\gamma}$. The benchmark scenario of table 1 is indicated by the blue dot. In the gray band, the thermal relic density of the lightest neutralino is consistent with the observed dark matter density. The yellow region is exluded by the XENON100 direct dark matter search, the red region is excluded by the Super-Kamiokande limit on the spin-dependent cross section of $\tilde{\chi}_1^0$.

It can be seen that, while $\tilde{\chi}_1^0$ is dominated by its singlino component in the depicted parameter space, a rather low M_2 is favorable in order to satisfy the direct detection

constraints. This is because the Higgs, which mediates the spin-independent interaction of $\tilde{\chi}_1^0$ with nucleons, mainly couples to the higgsino and singlino components of $\tilde{\chi}_1^0$ due to the relatively large λ and κ. An additional wino admixture tends to reduce $\sigma_p^{\rm SI}$. At the same time, the wino component of $\tilde{\chi}_1^0$ drives its annihilation into W pairs allowing for a thermal neutralino abundance which agrees with the dark matter abundance (gray band in figure 5). On the other hand, a light wino induces a splitting between the higgsino components of the lightest neutralino, N_{13} and N_{14}. This, in turn, enhances the spin-dependent cross section $\sigma_p^{\rm SD}$ (see section 5) resulting in the Super-Kamiokande excluded region at low M_2 and μ.[6] The annihilation of $\tilde{\chi}_1^0$ into γ-pairs is mediated by higgsinos in the loop, while winos do virtually not contribute due to the singlet nature of A_1. Therefore, $\langle\sigma v\rangle_{\gamma\gamma}$ grows with decreasing higgsino mass. Note, finally, that the direct and indirect detection constraints get weaker for smaller couplings λ and κ. In this case, however, one would need m_{A_1} closer to the resonance in order to keep $\langle\sigma v\rangle_{\gamma\gamma}$ large.

7   Summary

In this article we have shown that within the GNMSSM, a generalised version of the NMSSM, the experimental hints beyond the SM from the Fermi LAT telescope as well as from the LHC can be explained simultaneously while being consistent with all experimental constraints. As in the NMSSM the superpotential term $\lambda\,SH_uH_d$ plays a crucial role in this scheme: it drives the annihilation of the lightest neutralino into photons, induces new tree-level contributions to the mass of the light Higgs boson h and enhances the partial width of the decay $h \to \gamma\gamma$. To obtain a large enough annihilation cross section into photons, a very mild tuning of the pseudoscalar Higgs mass is required in the GNMSSM: it is sufficient to be within $\sim 20\,{\rm GeV}$ from the resonance. This is in contrast to the NMSSM, where the tuning is very substantial, because unlike in the GNMSSM a mainly singlino-like LSP is not possible, leading to much smaller effective couplings. Hence while the coupling λ is also present in the NMSSM, it is the additional flexibility in the mass spectrum of the GNMSSM which allows to simultaneously explain the Fermi γ ray line, ameliorate the little hierarchy problem, and explain a moderate excess in the $\gamma\gamma$-channel which is indicated by the Higgs searches of CMS and ATLAS.

To substantiate our claim we performed a thorough numerical analysis and presented an example point which features a $\sim 130\,{\rm GeV}$ lightest neutralino with an annihilation cross section into photons consistent with the indication from the Fermi satellite with

---

[6]To obtain the Super-Kamiokande limit on the spin-dependent cross section, we have weighted $\sigma_p^{\rm SI}$ by the fractional annihilation of $\tilde{\chi}_1^0$ into channels which induce hard neutrinos.

simultaneously the right relic abundance, a continuum photon spectrum consistent with observation, direct detection cross section below the experimental limits, electroweak observables consistent with experiment and a 125 GeV light Higgs boson with a slightly enhanced $h \to \gamma\gamma$ rate.

Acknowledgements

A   Mass matrices

If we decompose the complex Higgs fields and singlet after EWSB as

$$H_d^0 = \frac{1}{\sqrt{2}}\left(\phi_d + v_d + i\sigma_d\right) \tag{11}$$

$$H_u^0 = \frac{1}{\sqrt{2}}\left(\phi_u + v_u + i\sigma_u\right) \tag{12}$$

$$S = \frac{1}{\sqrt{2}}\left(\phi_s + v_s + i\sigma_s\right) \tag{13}$$

the mass matrices in the neutral Higgs sector read:

- Scalar Higgs. Basis: (ϕ_d, ϕ_u, ϕ_s)

$$
\begin{aligned}
m_{dd} = \frac{1}{8}\Big(& 4\big(2\mu + \sqrt{2}v_s\lambda\big)\mu^* + 4\big(\sqrt{2}v_s\mu + \big(v_s^2 + v_u^2\big)\lambda\big)\lambda^* \\
& + 8m_{H_d}^2 + \big(g_1^2 + g_2^2\big)\big(3v_d^2 - v_u^2\big)\Big)
\end{aligned} \tag{14}
$$

$$
\begin{aligned}
m_{ud} = \frac{1}{4}\Big(& -2v_s^2\Re\big(\lambda\kappa^*\big) - 4\Re\big(b\mu\big) + 4v_dv_u|\lambda|^2 \\
& - \big(g_1^2 + g_2^2\big)v_dv_u - \sqrt{2}v_s\big(2\Re\big(\lambda\mu_S^*\big) + 2\Re\big(\lambda A_\lambda\big)\big)\Big)
\end{aligned} \tag{15}
$$

$$
\begin{aligned}
m_{uu} = \frac{1}{8}\Big(& 4\big(2\mu + \sqrt{2}v_s\lambda\big)\mu^* + 4\big(\sqrt{2}v_s\mu + \big(v_d^2 + v_s^2\big)\lambda\big)\lambda^* + 8m_{H_u}^2 \\
& - \big(g_1^2 + g_2^2\big)\big(-3v_u^2 + v_d^2\big)\Big)
\end{aligned} \tag{16}
$$

$$
m_{sd} = -\frac{1}{4}v_u\Big(4v_s\Re\big(\lambda\kappa^*\big) + \sqrt{2}\big(2\Re\big(\lambda A_\lambda\big) + \mu_S\lambda^*\big) + \sqrt{2}\lambda\mu_S^*\Big)
$$

13

$$+ \frac{1}{\sqrt{2}} v_d \lambda \mu^* + v_d \left(\frac{1}{\sqrt{2}} \mu + v_s \lambda \right) \lambda^* \tag{17}$$

$$m_{su} = -\frac{1}{4} v_d \left(4 v_s \Re\left(\lambda \kappa^* \right) + \sqrt{2} \left(2\Re\left(\lambda A_\lambda \right) + \mu_S \lambda^* \right) + \sqrt{2} \lambda \mu_S^* \right) + \frac{1}{\sqrt{2}} v_u \lambda \mu^*$$

$$+ \left(\frac{1}{\sqrt{2}} v_u \mu + v_s v_u \lambda \right) \lambda^* \tag{18}$$

$$m_{ss} = \frac{1}{2} \left(6 v_s^2 |\kappa|^2 + v_d^2 |\lambda|^2 + v_u^2 |\lambda|^2 + 2\left(m_S^2 + |\mu_S|^2 + \Re\left(b_S \right) \right) \right.$$

$$\left. - 2 v_d v_u \Re\left(\lambda \kappa^* \right) + \sqrt{2} v_s \left(2\Re\left(\kappa A_\kappa \right) + 6\Re\left(\kappa \mu_S^* \right) \right) \right) \tag{19}$$

- Pseudoscalar Higgs. Basis: $(\sigma_d, \sigma_u, \sigma_s)$

$$m_{dd} = \frac{1}{8} \left(4\left(2\mu + \sqrt{2} v_s \lambda \right) \mu^* + 4\left(\sqrt{2} v_s \mu + \left(v_s^2 + v_u^2 \right) \lambda \right) \lambda^* \right. \tag{20}$$

$$\left. + 8 m_{H_d}^2 + \left(g_1^2 + g_2^2 \right) \left(- v_u^2 + v_d^2 \right) \right) \tag{21}$$

$$m_{ud} = \frac{1}{4} \left(4\Re\left(b\mu \right) + v_s \left(2 v_s \Re\left(\lambda \kappa^* \right) + \sqrt{2} \left(2\Re\left(\lambda \mu_S^* \right) + 2\Re\left(\lambda A_\lambda \right) \right) \right) \right) \tag{22}$$

$$m_{uu} = \frac{1}{8} \left(4\left(2\mu + \sqrt{2} v_s \lambda \right) \mu^* + 4\left(\sqrt{2} v_s \mu + \left(v_d^2 + v_s^2 \right) \lambda \right) \lambda^* \right. \tag{23}$$

$$\left. + 8 m_{H_u}^2 - \left(g_1^2 + g_2^2 \right) \left(- v_u^2 + v_d^2 \right) \right) \tag{24}$$

$$m_{sd} = -\frac{1}{4} v_u \left(4 v_s \Re\left(\lambda \kappa^* \right) + \sqrt{2} \left(- 2\Re\left(\lambda A_\lambda \right) + \mu_S \lambda^* \right) + \sqrt{2} \lambda \mu_S^* \right) \tag{25}$$

$$m_{su} = -\frac{1}{4} v_d \left(4 v_s \Re\left(\lambda \kappa^* \right) + \sqrt{2} \left(- 2\Re\left(\lambda A_\lambda \right) + \mu_S \lambda^* \right) + \sqrt{2} \lambda \mu_S^* \right) \tag{26}$$

$$m_{ss} = \frac{1}{2} \left(2 v_s^2 |\kappa|^2 + v_d^2 |\lambda|^2 + v_u^2 |\lambda|^2 + 2\left(- \Re\left(b_S \right) + m_S^2 \right. \right.$$

$$\left. \left. + |\mu_S|^2 \right) + 2 v_d v_u \Re\left(\lambda \kappa^* \right) + \sqrt{2} v_s \left(2\Re\left(\kappa \mu_S^* \right) - 2\Re\left(\kappa A_\kappa \right) \right) \right) \tag{27}$$

After eliminating the Goldstone mode, the mass matrix can be written as

$$M_{1,1} = \left(v_s(\sqrt{2}(A_\lambda + \mu_S) + v_s \kappa)\lambda + 2b\mu \right) / \sin(2\beta) \tag{28}$$

$$M_{1,2} = \frac{v}{\sqrt{2}} \lambda(A_\lambda - \sqrt{2} v_s \kappa - \mu_s) \tag{29}$$

$$M_{2,2} = -2 b_s - \frac{3}{\sqrt{2}} A_\kappa v_s \kappa - (v^2 \lambda \mu)/(\sqrt{2} v_s) - v_s \kappa \mu_s/\sqrt{2} - \sqrt{2} \xi_s / v_s$$

14

$$+ ((A_\lambda + \mu_s)\lambda v^2 \cos\beta \sin\beta)/(\sqrt{2}v_s) + 2v^2\kappa\lambda \cos\beta \sin\beta \tag{30}$$

The mass matrices of the charged Higgs as well as of the neutralinos and charginos are given by

- Charged Higgs. Basis: $\left(H_d^-, H_u^{+,*}\right)$

$$
\begin{aligned}
m_{dd} &= \frac{1}{8}\bigg(4\Big(2\mu + \sqrt{2}v_s\lambda\Big)\mu^* + 4v_s\Big(\sqrt{2}\mu + v_s\lambda\Big)\lambda^* + 8m_{H_d}^2 \\
&\quad + g_1^2\Big(-v_u^2 + v_d^2\Big) + g_2^2\Big(v_d^2 + v_u^2\Big)\bigg) \tag{31}
\end{aligned}
$$

$$
m_{ud} = \frac{1}{4}\Big(2v_s\Big(\sqrt{2}\Big(\lambda\mu_S^* + \lambda A_\lambda\Big) + v_s\lambda\kappa^*\Big) + 4b\mu - v_d v_u\Big(2|\lambda|^2 - g_2^2\Big)\Big) \tag{32}
$$

$$
\begin{aligned}
m_{uu} &= \frac{1}{8}\bigg(4\sqrt{2}v_s\lambda\mu^* + 4v_s\Big(\sqrt{2}\mu + v_s\lambda\Big)\lambda^* + 8m_{H_u}^2 \\
&\quad + 8|\mu|^2 + \Big(g_1^2 + g_2^2\Big)v_u^2 - g_1^2 v_d^2 + g_2^2 v_d^2\bigg) \tag{33}
\end{aligned}
$$

- Neutralino. Basis: $\left(\lambda_{\tilde{B}}, \tilde{W}^0, \tilde{H}_d^0, \tilde{H}_u^0, \tilde{S}\right)$

$$
m_N = \begin{pmatrix}
M_1 & 0 & -\frac{1}{2}g_1 v_d & \frac{1}{2}g_1 v_u & 0 \\
0 & M_2 & \frac{1}{2}g_2 v_d & -\frac{1}{2}g_2 v_u & 0 \\
-\frac{1}{2}g_1 v_d & \frac{1}{2}g_2 v_d & 0 & -\frac{1}{\sqrt{2}}v_s\lambda - \mu & -\frac{1}{\sqrt{2}}v_u\lambda \\
\frac{1}{2}g_1 v_u & -\frac{1}{2}g_2 v_u & -\frac{1}{\sqrt{2}}v_s\lambda - \mu & 0 & -\frac{1}{\sqrt{2}}v_d\lambda \\
0 & 0 & -\frac{1}{\sqrt{2}}v_u\lambda & -\frac{1}{\sqrt{2}}v_d\lambda & \sqrt{2}v_s\kappa + \mu_S
\end{pmatrix} \tag{34}
$$

- Chargino. Basis: $\left(\tilde{W}^-, \tilde{H}_d^-\right), \left(\tilde{W}^+, \tilde{H}_u^+\right)$

$$
m_{Ch} = \begin{pmatrix}
M_2 & \frac{1}{\sqrt{2}}g_2 v_u \\
\frac{1}{\sqrt{2}}g_2 v_d & \frac{1}{\sqrt{2}}v_s\lambda + \mu
\end{pmatrix} \tag{35}
$$

B   Couplings

- $\tilde{\chi}_i^0 \tilde{\chi}_j^0 A_k^h$

$$
\begin{aligned}
g^L_{\tilde{\chi}_i^0 \tilde{\chi}_j^0 A_k^h} =& \frac{1}{2}\Big(-g_2 N^*_{i2} N^*_{j3} Z^A_{k1} - \sqrt{2}\lambda N^*_{i5} N^*_{j4} Z^A_{k1} - \sqrt{2}\lambda N^*_{i4} N^*_{j5} Z^A_{k1} - g_1 N^*_{i4} N^*_{j1} Z^A_{k2} \\
&+ g_2 N^*_{i4} N^*_{j2} Z^A_{k2} - \sqrt{2}\lambda N^*_{i5} N^*_{j3} Z^A_{k2} + g_2 N^*_{i2} N^*_{j4} Z^A_{k2} \\
&+ g_1 N^*_{i1}\Big(N^*_{j3} Z^A_{k1} - N^*_{j4} Z^A_{k2} \Big) - \sqrt{2}\lambda N^*_{i4} N^*_{j3} Z^A_{k3} + 2\sqrt{2}\kappa N^*_{i5} N^*_{j5} Z^A_{k3} \\
&+ N^*_{i3}\Big(g_1 N^*_{j1} Z^A_{k1} - g_2 N^*_{j2} Z^A_{k1} - \sqrt{2}\lambda \Big(N^*_{j4} Z^A_{k3} + N^*_{j5} Z^A_{k2} \Big)\Big)\Big) \\
g^R_{\tilde{\chi}_i^0 \tilde{\chi}_j^0 A_k^h} =& -(g^L_{\tilde{\chi}_i^0 \tilde{\chi}_j^0 A_k^h})^* | (i \leftrightarrow j)
\end{aligned}
\tag{36}
$$

- $\tilde{\chi}_i^+ \tilde{\chi}_j^- A_k^h$

$$
\begin{aligned}
g^L_{\tilde{\chi}_i^+ \tilde{\chi}_j^- A_k^h} =& \frac{1}{\sqrt{2}}\Big(-g_2 U^*_{j1} V^*_{i2} Z^A_{k2} + U^*_{j2}\Big(-g_2 V^*_{i1} Z^A_{k1} + \lambda V^*_{i2} Z^A_{k3}\Big)\Big) \\
g^R_{\tilde{\chi}_i^+ \tilde{\chi}_j^- A_k^h} =& -(g^L_{\tilde{\chi}_i^+ \tilde{\chi}_j^- A_k^h})^* | (i \leftrightarrow j)
\end{aligned}
\tag{37}
$$

- $\tilde{\chi}_i^0 \tilde{\chi}_j^0 h_k$

$$
\begin{aligned}
g^L_{\tilde{\chi}_i^0 \tilde{\chi}_j^0 h_k} =& \frac{i}{2}\Big(-g_2 N^*_{i2} N^*_{j3} Z^H_{k1} + \sqrt{2}\lambda N^*_{i5} N^*_{j4} Z^H_{k1} + \sqrt{2}\lambda N^*_{i4} N^*_{j5} Z^H_{k1} - g_1 N^*_{i4} N^*_{j1} Z^H_{k2} \\
&+ g_2 N^*_{i4} N^*_{j2} Z^H_{k2} + \sqrt{2}\lambda N^*_{i5} N^*_{j3} Z^H_{k2} + g_2 N^*_{i2} N^*_{j4} Z^H_{k2} \\
&+ g_1 N^*_{i1}\Big(N^*_{j3} Z^H_{k1} - N^*_{j4} Z^H_{k2} \Big) + \sqrt{2}\lambda N^*_{i4} N^*_{j3} Z^H_{k3} - 2\sqrt{2}\kappa N^*_{i5} N^*_{j5} Z^H_{k3}\Big) \\
g^R_{\tilde{\chi}_i^0 \tilde{\chi}_j^0 h_k} =& -(g^L_{\tilde{\chi}_i^0 \tilde{\chi}_j^0 h_k})^* | (i \leftrightarrow j)
\end{aligned}
\tag{38}
$$

- $\tilde{\chi}_i^0 \tilde{\chi}_j^0 Z$

$$
\begin{aligned}
g^L_{\tilde{\chi}_i^0 \tilde{\chi}_j^0 Z} =& -\frac{i}{2}\Big(g_1 \sin\Theta_W + g_2 \cos\Theta_W \Big)\Big(N^*_{j3} N_{i3} - N^*_{j4} N_{i4}\Big) \\
g^R_{\tilde{\chi}_i^0 \tilde{\chi}_j^0 Z} =& (g^L_{\tilde{\chi}_i^0 \tilde{\chi}_j^0 Z})^*
\end{aligned}
\tag{39}
$$

References

[1] ATLAS Collaboration, ATLAS-CONF-2012-093.

[2] CMS Collaboration, CMS-PAS-HIG-12-020.

[3] U. Ellwanger, JHEP **1203** (2012), 044, [1112.3548].

[4] J.-J. Cao, Z.-X. Heng, J. M. Yang, Y.-M. Zhang, and J.-Y. Zhu, JHEP **1203** (2012), 086, [1202.5821].

[5] V. Barger, M. Ishida, and W.-Y. Keung, (2012), 1207.0779.

[6] M. Carena, I. Low, and C. E. Wagner, (2012), 1206.1082.

[7] D. S. Alves, P. J. Fox, and N. J. Weiner, (2012), 1207.5499.

[8] N. Bonne and G. Moreau, (2012), 1206.3360.

[9] B. Bellazzini, C. Petersson, and R. Torre, (2012), 1207.0803.

[10] M. R. Buckley and D. Hooper, (2012), 1207.1445.

[11] H. An, T. Liu, and L.-T. Wang, (2012), 1207.2473.

[12] A. G. Cohen and M. Schmaltz, (2012), 1207.3495.

[13] A. Alves, A. Dias, E. R. Barreto, C. S. Pires, F. S. Queiroz, et al., (2012), 1207.3699.

[14] A. Joglekar, P. Schwaller, and C. E. Wagner, (2012), 1207.4235.

[15] N. Haba, K. Kaneta, Y. Mimura, and R. Takahashi, (2012), 1207.5102.

[16] L. G. Almeida, E. Bertuzzo, P. A. Machado, and R. Z. Funchal, (2012), 1207.5254.

[17] R. Benbrik, M. G. Bock, S. Heinemeyer, O. Stal, G. Weiglein, et al., (2012), 1207.1096.

[18] N. Arkani-Hamed, K. Blum, R. T. D'Agnolo, and J. Fan, (2012), 1207.4482.

[19] K. Schmidt-Hoberg and F. Staub, (2012), 1208.1683.

[20] M. Chala, (2012), 1210.6208.

[21] T. Bringmann, X. Huang, A. Ibarra, S. Vogl, and C. Weniger, JCAP **1207** (2012), 054, [1203.1312].

[22] C. Weniger, (2012), 1204.2797.

17

[23] S. Profumo and T. Linden, JCAP **1207** (2012), 011, [1204.6047].

[24] F. Aharonian, D. Khangulyan, and D. Malyshev, (2012), 1207.0458.

[25] M. Su and D. P. Finkbeiner, (2012), 1206.1616.

[26] T. Bringmann and C. Weniger, (2012), 1208.5481.

[27] M. Kuhlen, J. Guedes, A. Pillepich, P. Madau, and L. Mayer, (2012), 1208.4844.

[28] A. Albert, Talk at the Fermi Symposium 2012.

[29] E. Tempel, A. Hektor, and M. Raidal, (2012), 1205.1045.

[30] A. Hektor, M. Raidal, and E. Tempel, (2012), 1209.4548.

[31] D. P. Finkbeiner, M. Su, and C. Weniger, (2012), 1209.4562.

[32] R. Laha, K. C. Y. Ng, B. Dasgupta, and S. Horiuchi, (2012), 1208.5488.

[33] G. Chalons, (2012), 1204.4591.

[34] G. Chalons and A. Semenov, JHEP **1112** (2011), 055, [1110.2064].

[35] A. Ibarra, S. Lopez Gehler, and M. Pato, (2012), 1205.0007.

[36] E. Dudas, Y. Mambrini, S. Pokorski, and A. Romagnoni, (2012), 1205.1520.

[37] J. M. Cline, (2012), 1205.2688.

[38] K.-Y. Choi and O. Seto, (2012), 1205.3276.

[39] B. Kyae and J.-C. Park, (2012), 1205.4151.

[40] H. M. Lee, M. Park, and W.-I. Park, (2012), 1205.4675.

[41] A. Rajaraman, T. M. Tait, and D. Whiteson, (2012), 1205.4723.

[42] M. R. Buckley and D. Hooper, (2012), 1205.6811.

[43] X. Chu, T. Hambye, T. Scarna, and M. H. Tytgat, (2012), 1206.2279.

[44] D. Das, U. Ellwanger, and P. Mitropoulos, JCAP **1208** (2012), 003, [1206.2639].

[45] Z. Kang, T. Li, J. Li, and Y. Liu, (2012), 1206.2863.

[46] N. Weiner and I. Yavin, (2012), 1206.2910.

[47] W. Buchmuller and M. Garny, (2012), 1206.7056.

[48] M. T. Frandsen, U. Haisch, F. Kahlhoefer, P. Mertsch, and K. Schmidt-Hoberg, JCAP **1210** (2012), 033, [1207.3971].

[49] F. D'Eramo, M. McCullough, and J. Thaler, (2012), 1210.7817.

[50] T. Cohen, M. Lisanti, T. R. Slatyer, and J. G. Wacker, JHEP **1210** (2012), 134, [1207.0800].

[51] I. Cholis, M. Tavakoli, and P. Ullio, Phys.Rev. **D86** (2012), 083525, [1207.1468].

[52] G. G. Ross and K. Schmidt-Hoberg, (2011), 1108.1284.

[53] H. M. Lee et al., Phys. Lett. **B694** (2011), 491–495, [1009.0905].

[54] H. M. Lee et al., Nucl. Phys. **B850** (2011), 1–30, [1102.3595].

[55] G. G. Ross, K. Schmidt-Hoberg, and F. Staub, (2012), 1205.1509.

[56] M. Maniatis, Int.J.Mod.Phys. **A25** (2010), 3505–3602, [0906.0777].

[57] U. Ellwanger, C. Hugonie, and A. M. Teixeira, Phys. Rept. **496** (2010), 1–77, [0910.1785].

[58] M. Bastero-Gil, C. Hugonie, S. King, D. Roy, and S. Vempati, Phys.Lett. **B489** (2000), 359–366, [hep-ph/0006198].

[59] R. Dermisek and J. F. Gunion, Phys.Rev. **D73** (2006), 111701, [hep-ph/0510322].

[60] R. Dermisek, J. F. Gunion, and B. McElrath, Phys.Rev. **D76** (2007), 051105, [hep-ph/0612031].

[61] R. Dermisek and J. F. Gunion, Phys.Rev. **D76** (2007), 095006, [0705.4387].

[62] U. Ellwanger, G. Espitalier-Noel, and C. Hugonie, (2011), 1107.2472.

[63] L. J. Hall, D. Pinner, and J. T. Ruderman, (2011), 1112.2703.

[64] L. Bergstrom and P. Ullio, Nucl.Phys. **B504** (1997), 27–44, [hep-ph/9706232].

[65] Z. Bern, P. Gondolo, and M. Perelstein, Phys.Lett. **B411** (1997), 86–96, [hep-ph/9706538].

[66] XENON100 Collaboration, E. Aprile et al., Phys.Rev.Lett. **109** (2012), 181301, [1207.5988].

[67] P. Ullio and L. Bergstrom, Phys.Rev. **D57** (1998), 1962–1971, [hep-ph/9707333].

[68] G. Belanger, F. Boudjema, A. Pukhov, and A. Semenov, Comput.Phys.Commun. **180** (2009), 747–767, [0803.2360].

[69] R. Kappl, M. Ratz, and M. W. Winkler, Phys.Lett. **B695** (2011), 169–173, [1010.0553].

[70] Super-Kamiokande Collaboration, T. Tanaka et al., Astrophys.J. **742** (2011), 78, [1108.3384].

[71] R. Kappl and M. W. Winkler, Nucl.Phys. **B850** (2011), 505–521, [1104.0679].

[72] IceCube Collaboration, R. Abbasi et al., Phys.Rev. **D85** (2012), 042002, [1112.1840].

[73] Fermi-LAT collaboration, M. Ackermann et al., Phys.Rev.Lett. **107** (2011), 241302, [1108.3546].

[74] PAMELA Collaboration, O. Adriani et al., Phys.Rev.Lett. **105** (2010), 121101, [1007.0821].

[75] F. Donato, D. Maurin, P. Brun, T. Delahaye, and P. Salati, Phys.Rev.Lett. **102** (2009), 071301, [0810.5292].

[76] K. Abe, H. Fuke, S. Haino, T. Hams, M. Hasegawa, et al., Phys.Rev.Lett. **108** (2012), 051102, [1107.6000].

[77] R. Kappl and M. W. Winkler, Phys.Rev. **D85** (2012), 123522, [1110.4376].

[78] W. Porod, Comput.Phys.Commun. **153** (2003), 275–315, [hep-ph/0301101].

[79] W. Porod and F. Staub, (2011), 1104.1573.

[80] F. Staub, (2008), 0806.0538.

[81] F. Staub, Comput.Phys.Commun. **181** (2010), 1077–1086, [0909.2863].

[82] F. Staub, Comput.Phys.Commun. **182** (2011), 808–833, [1002.0840].

[83] F. Staub, (2012), 1207.0906.

[84] D. M. Pierce, J. A. Bagger, K. T. Matchev, and R.-j. Zhang, Nucl.Phys. **B491** (1997), 3–67, [hep-ph/9606211].

[85] F. Staub, W. Porod, and B. Herrmann, JHEP **1010** (2010), 040, [1007.4049].

[86] A. Dedes, G. Degrassi, and P. Slavich, Nucl.Phys. **B672** (2003), 144–162, [hep-ph/0305127].

[87] A. Dedes and P. Slavich, Nucl.Phys. **B657** (2003), 333–354, [hep-ph/0212132].

[88] A. Brignole, G. Degrassi, P. Slavich, and F. Zwirner, Nucl.Phys. **B643** (2002), 79–92, [hep-ph/0206101].

[89] A. Brignole, G. Degrassi, P. Slavich, and F. Zwirner, Nucl.Phys. **B631** (2002), 195–218, [hep-ph/0112177].

[90] M. Spira, A. Djouadi, D. Graudenz, and P. Zerwas, Nucl.Phys. **B453** (1995), 17–82, [hep-ph/9504378].

[91] G. Belanger, F. Boudjema, A. Pukhov, and A. Semenov, Comput.Phys.Commun. **176** (2007), 367–382, [hep-ph/0607059].

[92] G. Belanger, F. Boudjema, A. Pukhov, and A. Semenov, Comput.Phys.Commun. **177** (2007), 894–895.

[93] G. Belanger, F. Boudjema, A. Pukhov, and A. Semenov, (2010), 1005.4133.

[94] A. Pukhov, (2004), hep-ph/0412191.

[95] G. Belanger, N. D. Christensen, A. Pukhov, and A. Semenov, Comput.Phys.Commun. **182** (2011), 763–774, [1008.0181].

[96] C. Y. Pages, 'SM Higgs Branching Ratios and Partial-Decay Widths, [twiki.cern.ch/twiki/bin/view/LHCPhysics/CERNYellowReportPageBR2].

[97] ATLAS Collaboration, ATLAS-CONF-2012-154.

[98] CMS Collaboration, CMS-SUS-12-022.

Input			
$\tan\beta$	1.2	v_s [GeV]	-4.0
λ	0.74	A_λ [GeV]	0
κ	1.4	A_κ [GeV]	0
μ_s [GeV]	103.0	b_s [GeV^2]	$3.356 \cdot 10^5$
μ [GeV]	280.0	$b\mu$ [GeV^2]	$2.4 \cdot 10^5$
M_1 [GeV]	1500.0	M_2 [GeV]	193.0
M_3 [GeV]	1500.0	m_{scalar} [GeV]	1500.0
$A_{top}Y_{top}$ [GeV]	1500.0	ξ_S [GeV^3]	0.0
CP even Higgs sector			
m_{h_1} [GeV]	125.7	down fraction h_1	41.5%
m_{h_2} [GeV]	690.1	up fraction h_1	57.8%
m_{h_3} [GeV]	786.8	singlet fraction h_1	0.7%
CP odd Higgs sector			
m_{A_1} [GeV]	247.5	singlet fraction A_1	99.9%
m_{A_2} [GeV]	691.9	up and down fraction A_1	0.1%
Neutralino sector			
$\tilde\chi_1^0$ [GeV]	130.0	bino fraction $\tilde\chi_1^0$	<0.1%
$\tilde\chi_2^0$ [GeV]	156.4	wino fraction $\tilde\chi_1^0$	5.1%
$\tilde\chi_3^0$ [GeV]	316.2	down-higgsino fraction $\tilde\chi_1^0$	0.3%
$\tilde\chi_4^0$ [GeV]	331.6	up-higgsino fraction $\tilde\chi_1^0$	10.0%
$\tilde\chi_5^0$ [GeV]	1497.4	singlet fraction $\tilde\chi_1^0$	84.5%
Chargino sector			
$\tilde\chi_1^+$ [GeV]	154.8	wino fraction $\tilde\chi_1^+$	70.6%
$\tilde\chi_2^+$ [GeV]	332.6	higgsino fraction $\tilde\chi_1^+$	29.4%
Electroweak observables			
$R_{\gamma\gamma}$	1.2	$R_{b\bar b}$	1.0
R_{ZZ}	1.0	$R_{\tau\bar\tau}$	1.0
$\mathrm{Br}(b \to s\gamma)$	$3.4 \cdot 10^{-4}$	$\mathrm{Br}(B_s \to \mu\mu)$	$3.7 \cdot 10^{-9}$
Δa_μ	$-1.2 \cdot 10^{-11}$	$\delta\rho$	$4.5 \cdot 10^{-5}$
Dark matter			
Ωh^2	0.1	X_{FO}	24.9
σ_p^{SI} [cm^2]	$2.2 \cdot 10^{-45}$	σ_p^{SD} [cm^2]	$3.8 \cdot 10^{-40}$
$\langle\sigma v\rangle_{\gamma\gamma}$ [cm^3/s]	$0.83 \cdot 10^{-27}$	$\langle\sigma v\rangle_{\gamma Z}$ [cm^3/s]	$0.79 \cdot 10^{-27}$

Table 1: Benchmark point for the GNMSSM. R_{XY} denotes the production cross section of $pp \to h \to XY$ normalised to the SM expectations (based on the values of the CERN yellow pages [96]).